Applied Numerical Mathematics 105 (2016) 47–63

Contents lists available at ScienceDirect

Applied Numerical Mathematics

www.elsevier.com/locate/apnum

A path-conservative Osher-type scheme for axially symmetric compressible flows in flexible visco-elastic tubes

Julia Leibinger [a], Michael Dumbser [b,*], Uwe Iben [a], Isabell Wayand [a]

[a] Robert Bosch GmbH, Robert-Bosch-Campus 1, 71272 Renningen, Germany
[b] Department of Civil, Environmental and Mechanical Engineering, University of Trento, Via Mesiano 77, 38123 Trento, Italy

ARTICLE INFO

Article history:
Received 15 October 2015
Received in revised form 29 January 2016
Accepted 5 February 2016
Available online 10 February 2016

Keywords:
Compressible flows in compliant tubes
Flexible ducts with variable cross section
Fluid–structure interaction (FSI)
Visco-elastic wall behavior
Non-conservative hyperbolic systems
Well-balanced path-conservative finite volume schemes

ABSTRACT

Flexible tubes are widely used in modern industrial hydraulic systems as connections between different components like valves, pumps and actuators. For the design and the analysis of the temporal behavior of a hydraulic system, one therefore needs an accurate mathematical model that describes the fluid flow in a compliant duct. Hence, in this paper we want to model the fluid–structure-interaction (FSI) problem given by the axially symmetric flow of a compressible barotropic fluid that flows through flexible tubes made of vulcanized rubber. The material of the tube can be described by using a visco-elastic rheology, which takes into account the strain relaxation of the material. The resulting mathematical model consists in a one-dimensional system of nonlinear hyperbolic partial differential equations (PDE) with non-conservative products and algebraic source terms. To solve this system numerically, we apply the DOT method, which is a generalized path-conservative Osher-type Riemann solver for conservative and non-conservative hyperbolic PDE recently proposed in [23] and [22].

We provide numerical evidence that the proposed DOT Riemann solver is *well-balanced* for the governing PDE system under consideration. The method is compared to available quasi-exact solutions of the Riemann problem in the case of an elastic wall described by the Laplace law. It is also compared to available experimental data and exact solutions obtained in the frequency domain for a linear visco-elastic wall behavior. In all cases under investigation the proposed path-conservative finite volume scheme based on the DOT Riemann solver is able to produce very accurate results.

1. Introduction

Nowadays there exist many important industrial hydraulic systems that require an accurate mathematical modeling of the system behavior already at the design stage. Especially in the automotive industry there are, for example, the braking systems and the fuel injection into the combustion engine. As these systems get more and more complex, and since they should be more and more efficient due to increased safety standards or an increasingly restrictive environmental legislation, one needs to understand each single component as well as the entire hydraulic system and the interaction between the different components. When one wants to understand the dynamic behavior of the system already at the design stage, an important tool is its mathematical modeling and the subsequent numerical simulation.

* Corresponding author.
E-mail addresses: julia.leibinger@de.bosch.com (J. Leibinger), michael.dumbser@unitn.it (M. Dumbser), uwe.iben@de.bosch.com (U. Iben).

http://dx.doi.org/10.1016/j.apnum.2016.02.001
0168-9274/

Since flexible tubes are used in many hydraulic systems for the connection of different components, it is very important to understand and simulate their behavior. Therefore one needs a model for the physical effects occurring in the fluid as well as in the surrounding elastic tube. The fluid can be modeled by the one-dimensional cross-sectionally averaged compressible Euler equations in a duct with variable cross section, see [31,44]. Hooke's law has been used in the past [24] for the description of the elasticity of the tube wall, as well as the law of Laplace [13]. But when comparing the numerical results obtained with these simplified laws to experimental results of a flexible polymer tube, one can see that there is not enough dissipation in the system. So the next step was to use a visco-elastic model. Such models consist of dashpots and springs, so that they can reproduce the elastic as well as the viscous behavior of the wall material. Such models are for example described in [32].

In this paper we therefore want to model the fluid–structure-interaction (FSI) problem given by the axially symmetric flow of a compressible barotropic fluid through flexible polymer tubes. Hence, we present two different elasticity models—a simple Laplace law and a the widely used Maxwell model that is capable of reproducing visco-elastic effects of the polymer material [27]. In combination with the Euler equations for the flow of a compressible fluid in flexible tubes, we get a system of non-conservative hyperbolic partial differential equations (PDE).

To solve this non-conservative PDE system we employ the family of path-conservative schemes developed by Castro & Parés and co-workers [10,43,7,25,8,37,12,18,19,17], which are based on the theory of Dal Maso, Le Floch and Murat [36] on weak solutions for hyperbolic PDE with non-conservative products. The family of path-conservative schemes can be seen as a generalization of the weak formulation of the Roe method proposed by Toumi [46] and of the wave-propagation algorithm of LeVeque [35,34] for PDE with source terms. We would like to stress that there are still unresolved problems related to the choice of the path for general non-conservative PDE, which have been discussed in detail in [11].

In the following, we use a generalized version of the Riemann solver of Osher and Solomon [42] for conservative and non-conservative hyperbolic PDE recently proposed by Dumbser and Toro [23,22] (DOT). Note that the DOT solver can be further simplified in the context of polynomial viscosity methods (PVM), as recently described in [9]. We also would like to refer the reader to the successful use of path-conservative finite volume schemes based on the DOT Riemann solver in the context of computational hemodynamics, see the work of Müller & Toro et al. [39–41,38], where very recently the flow of an incompressible fluid in a network of compliant blood vessels has been considered. The present scheme is meant to be an alternative discretization of compressible flows in compliant ducts based on *explicit* path-conservative Godunov-type finite volume schemes, compared to the *semi-implicit* finite-volume and finite-difference discretization of such flows presented in [20]. The theoretical framework of these nonlinear semi-implicit schemes was presented in the papers by Brugnano and Casulli [4–6] and Casulli and Zanolli [14,15]. From the conceptual point of view, there are several important differences between the semi-implicit approach [20], and the path-conservative Godunov-type method presented here, which we briefly discuss in the following. The semi-implicit finite volume scheme [20] has to obey only a very mild CFL condition that is based on the *flow velocity*, while the explicit path-conservative scheme used here has to obey a more stringent CFL stability condition based on the *effective sound speed* of the coupled fluid–structure system. This makes the semi-implicit scheme [20] particularly suitable and computationally efficient for low Mach number and quasi-incompressible flows. In contrast, the second order shock capturing path-conservative Osher-type scheme presented here is more accurate and more efficient in the presence of strong shock waves and other discontinuities, since the DOT solver is a little dissipative and complete Riemann solver and since in the case of high Mach number flows, the flow velocity and the effective sound speed of the coupled fluid–structure system are rather close to each other. However, the main goal of this paper is not a detailed comparison with the method proposed in [20], but to provide an alternative discretization based on completely different design principles.

The rest of this paper is structured as follows: first, we present the set of equations that describes a compressible barotropic fluid flowing through a flexible visco-elastic tube with variable cross section. We assume an axially symmetric hydrostatic flow, where the fluid pressure is constant within each cross section. The governing PDE system is hyperbolic, with a conservative and a non-conservative part. In section 3 we present the Riemann solver that is used as a building block of the path-conservative finite volume scheme. In section 4 we provide some numerical results. The numerical scheme is applied to some classical Riemann problems for which a quasi-exact solution has been derived in [20,21]. We then simulate the dynamic behavior of a compressible fluid flowing through a flexible visco-elastic tube for which an exact solution exists in the frequency domain and for which also experimental data are available. The paper is rounded-off with some concluding remarks and an outlook to future research in section 5.

2. The governing PDE system of the coupled FSI problem

In the following section we introduce the PDE describing the flow of a barotropic fluid through a flexible tube, together with the visco-elastic behavior of the tube wall.

2.1. The cross-sectionally averaged Euler equations for the fluid

The axially symmetric flow of a compressible fluid through a tube with variable cross section $A(x,t)$ is modeled by the 1D cross-sectionally averaged Euler equations. We assume a barotropic fluid and a hydrostatic pressure that is constant within each cross section. The governing equations for the fluid read:

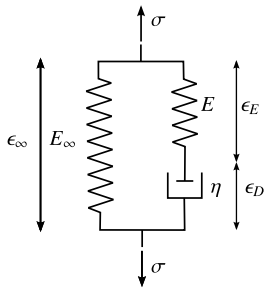

Fig. 1. Schematic representation of a 3-parameter Maxwell model.

$$\frac{\partial}{\partial t}(A\rho) + \frac{\partial}{\partial x}(A\rho u) = 0, \tag{1}$$

$$\frac{\partial}{\partial t}(A\rho u) + \frac{\partial}{\partial x}(A\rho u^2 + Ap) - p\frac{\partial A}{\partial x} = F_R. \tag{2}$$

Within these partial differential equations (PDE) ρ is the cross-sectional average of the fluid density, p is the averaged fluid pressure, u is the averaged fluid velocity and F_R is a model for the friction between the fluid and the tube wall, see [47].

Since we assume a barotropic fluid, the fluid pressure only depends on the density, hence $p = p(\rho)$. The entropy production due to turbulence and friction as well as wall motion is neglected. The equation of state also takes into account the two-phase flow caused by cavitation. Cavitation in a flowing liquid occurs when the pressure inside the tube drops below the saturated vapor pressure p_v. The model we use is quite simple and the state inside the tube is averaged. This means that we assume an averaged pressure and not a separate fluid and vapor pressure. So there is no information of bubble size or distribution, which occur during the cavitation process. For the density the following homogeneous mixture approximation is used, see also [20]:

$$\rho(p) = \begin{cases} \rho_0 + \frac{1}{c_0^2}(p - p_v), & \text{if } p \geq p_v, \\ \frac{1}{\frac{\mu(p)}{\rho_V(p)} + \frac{1-\mu(p)}{\rho_0}}, & \text{if } 0 < p < p_v, \end{cases} \tag{3}$$

with the reference density ρ_0 and the speed of sound c_0 at reference conditions, the mass fraction of the vapor $\mu(p) = -K(p - p_v)$, the cavitation constant K and the vapor density $\rho_v(p) = \frac{p}{R_v T_0}$ calculated with the ideal gas law, where R_v are the specific gas constant and T_0 is a reference temperature.

As an addition to these equations we need a model for the visco-elastic behavior of the tube wall. In the following we will consider two different models – the simple Laplace law and a more sophisticated Maxwell model.

2.2. Material model for the visco-elastic tube wall

As we want to consider flexible tubes we need to take into account the movement of the tube wall. This is done with two different models – a simple Laplace law and a more complex Maxwell model. With the Laplace law we can validate the correctness of the numerical scheme by comparing the numerical solution to a quasi-exact solution of one-dimensional shock tube problems, whereas the Maxwell model is necessary to reproduce the dynamic behavior of flexible visco-elastic tubes used in real industrial applications.

2.2.1. The Laplace law

An easy way to model the compliance of the tube wall is the Laplace law, where the cross-sectional area A only depends linearly on the pressure p, i.e.

$$A = A_0 + \frac{1}{\beta}(p - p_{ext}), \tag{4}$$

where A_0 is the cross-sectional area of the tube in equilibrium, β is an elasticity constant and p_{ext} is the equilibrium pressure.

2.2.2. The Maxwell model

To model a realistic polymer material, the visco-elasticity of the material needs to be included into the model. Therefore we use the generalized three-parameter Maxwell model like in [32]. This model combines springs and dashpots to take into account the elasticity and the time dependent relaxation of the wall material. In Fig. 1 the connection of the springs and the dashpots in series and in parallel is shown.

With this model system we obtain the following equations for the basic stress-strain relations:

$$
\begin{aligned}
\epsilon &= \epsilon_\infty = \epsilon_E + \epsilon_D \\
\sigma &= \sigma_\infty + \sigma_R = \sigma_\infty + \sigma_E = \sigma_\infty + \sigma_D \\
\sigma_R &= \sigma_E = \sigma_D \\
\sigma_E &= E\epsilon_E = E(\epsilon - \epsilon_D) \\
\sigma_\infty &= E_\infty \epsilon_\infty = E_\infty \epsilon \\
\sigma_D &= \eta \dot{\epsilon}_D \\
\Rightarrow \dot{\epsilon_D} &= \frac{\sigma_D}{\eta} = \frac{\sigma_E}{\eta} = \frac{E(\epsilon - \epsilon_E)}{\eta},
\end{aligned} \tag{5}
$$

with the stresses σ, the strains ϵ, the elasticity moduli E and the damping parameter η.

With these equations the balance of forces of the 3-parameter Maxwell model is described as follows:

$$\sigma = \sigma_\infty + \sigma_E = \epsilon E_\infty + \epsilon_E E = \epsilon E_\infty + (\epsilon - \epsilon_D)E.$$

Differentiating the above equation leads to

$$
\begin{aligned}
\dot{\sigma} &= \dot{\epsilon}(E_\infty + E) - \dot{\epsilon}_D E \\
&= \dot{\epsilon}(E_\infty + E) - \frac{E}{\eta}\sigma_D \\
&= \dot{\epsilon}(E_\infty + E) - \frac{E}{\eta}(\sigma - E_\infty \epsilon).
\end{aligned} \tag{6}
$$

To close the system of equations and to couple the structure to the force obtained from the fluid, we need to relate the pressure of the fluid to the strain in the tube wall. This is done by applying Barlow's formula:

$$\sigma = \frac{r}{h}(p - p_{ext}) = W(p - p_{ext}), \tag{7}$$

with r the pipe radius, h the thickness of the pipe wall and the parameter $W = r/h$, which depends on the radius and the thickness of the pipe wall. In addition, we need a kinematic relation between the strain ϵ and the cross sectional area of the pipe A:

$$\phi = \frac{A}{A_0} = \left(\frac{r}{r_0}\right)^2 = \left(\frac{r_0 + \Delta r}{r_0}\right)^2 = (1 + \epsilon)^2. \tag{8}$$

With the equations (6), (7) and a linearized version of equation (8) for small ϵ we obtain the following differential equation for the normalized cross sectional area of the pipe (see [27]):

$$\frac{\partial \phi}{\partial t} = -\frac{1}{\frac{E_0 \phi}{2Wc^2} + \rho}\frac{\partial(\phi \rho u)}{\partial x} + \frac{(2W(p - p_{ext}) - (\phi - 1)E_\infty)\phi}{\tau_1(2Wc^2\rho + E_0\phi)}, \tag{9}$$

where $c = \sqrt{\partial p / \partial \rho}$ is the speed of sound of the fluid, $\tau = \frac{\eta}{E}$ is the relaxation parameter and $E_0 = E_\infty + E$.

2.3. The coupled system of the fluid–structure-interaction problem

The equations for the material models, as characterized in the last section 2.2, have to be added to the cross-sectionally averaged Euler equations as described in equations (1) and (2). We thus obtain:

$$\frac{\partial}{\partial t}(A\rho) + \frac{\partial}{\partial x}(A\rho u) = 0, \tag{10}$$

$$\frac{\partial}{\partial t}(A\rho u) + \frac{\partial}{\partial x}(A\rho u^2 + Ap) - p\frac{\partial A}{\partial x} = F_R, \tag{11}$$

$$\frac{\partial}{\partial t}A + d\frac{\partial}{\partial x}(A\rho u) = S, \tag{12}$$

$$\frac{\partial}{\partial t}(A_0) = 0. \tag{13}$$

Equation (12) is a unified formulation for both wall models. In the following we will define the corresponding terms d and S for the Laplace law and for the 3-parameter Maxwell body, respectively. The last equation (13) states that the spatially variable equilibrium cross section A_0 is constant in time.

2.3.1. Laplace law

To get the requested formulation for the Laplace law, we need to differentiate equation (4) with respect to t and obtain

$$\frac{\partial A}{\partial t} = \frac{1}{\beta}\frac{\partial p}{\partial t} = \frac{1}{\beta}\frac{\partial p}{\partial \rho}\frac{\partial \rho}{\partial t}, \tag{14}$$

with $\frac{\partial p}{\partial \rho} = c^2$. Employing the product rule for $\frac{\partial}{\partial t} A\rho$ and using equation (10), we get

$$\frac{\partial A}{\partial t} = -\frac{c^2}{\beta A + \rho c^2}\frac{\partial (A\rho u)}{\partial x}, \tag{15}$$

hence the values d and S from (12)

$$d = \frac{1}{\frac{\beta A}{c^2} + \rho} \qquad \text{and} \qquad S = 0. \tag{16}$$

2.3.2. Maxwell model

The Maxwell equation (9) already has the required form. Therefore the terms d and S in Eqn. (12) read

$$d = \frac{1}{\frac{E_0 \phi}{2Wc^2} + \rho} \qquad \text{and} \qquad S = \frac{(2W(p - p_{ext}) - (\phi - 1)E_\infty)\, A}{\tau(2Wc^2\rho + E_0\phi)}. \tag{17}$$

When we want to describe thick-walled tubes ($r_a/r_i > 1.2$) the Barlow formula (7) is no longer valid. Hence, a different wall geometry parameter W is needed, which approximates the stress at the inner tube wall like in [33,2],

$$W = 2\frac{\left(\frac{r_a}{r_i}\right)(1+\nu) + 1 - 2\nu}{\left(\frac{r_a}{r_i}\right)^2 - 1}, \tag{18}$$

where r_a is the outer wall radius and r_i is the inner radius.

3. The DOT Riemann solver

For solving the PDE system described in the Sec. 2, an Osher-type Riemann solver is used, which has been proposed by Dumbser and Toro in [23,22] (so-called DOT Riemann solver). The method is applicable to hyperbolic systems of PDE with a conservative and a non-conservation part that can be written in the following general form:

$$\frac{\partial \mathbf{Q}}{\partial t} + \frac{\partial}{\partial x}\mathbf{f}(\mathbf{Q}) + \mathbf{B}(\mathbf{Q})\frac{\partial \mathbf{Q}}{\partial x} = \mathbf{S}(\mathbf{Q}), \tag{19}$$

where $\mathbf{Q} = \mathbf{Q}(x,t) \in \Omega_{\mathbf{Q}} \subset \mathbb{R}^m$ is the state vector, $\mathbf{f}$ is a nonlinear flux that contains the conservative part and $\mathbf{B}(\mathbf{Q})$ is an $m \times m$ matrix that includes the purely non-conservative part of the system. $\mathbf{S}(\mathbf{Q})$ is a nonlinear algebraic source term that takes into account the wall friction F_R and the term S of the Maxwell model for the visco-elastic wall. The system (19) can be equivalently written in the following quasi-linear form

$$\frac{\partial \mathbf{Q}}{\partial t} + \mathbf{A}(\mathbf{Q})\frac{\partial \mathbf{Q}}{\partial x} = \mathbf{S}(\mathbf{Q}), \tag{20}$$

with the system matrix $\mathbf{A}(\mathbf{Q}) = \partial \mathbf{f}/\partial \mathbf{Q} + \mathbf{B}(\mathbf{Q})$. The system (20) and therefore also the system (19) is called *hyperbolic*, if the matrix $\mathbf{A}(\mathbf{Q})$ is diagonalizable, i.e. $\mathbf{A}(\mathbf{Q}) = \mathbf{R}(\mathbf{Q})\mathbf{\Lambda}(\mathbf{Q})\mathbf{R}^{-1}(\mathbf{Q})$ with a diagonal matrix $\mathbf{\Lambda}(\mathbf{Q}) = \mathrm{diag}(\lambda_1, \ldots, \lambda_i, \ldots \lambda_m)$ containing only real eigenvalues λ_i and a complete set of linearly independent right eigenvectors $\mathbf{R}(\mathbf{Q})$. We first briefly review the DOT Riemann solver and subsequently apply it to the governing PDE system of our fluid–structure interaction problem (10)–(13).

3.1. Review of the DOT solver for nonlinear hyperbolic conservation laws

First, we look at the purely conservative part of the hyperbolic system. A simple reformulation of the Riemann solver of Osher and Solomon for general nonlinear systems of hyperbolic conservation laws is described in [22]. In the case of Eqn. (19) without non-conservative terms and without source terms, we have $\mathbf{B}(\mathbf{Q}) = 0$ and $\mathbf{S}(\mathbf{Q}) = 0$. The system then takes the simpler form of a *conservation law* and reads

$$\frac{\partial \mathbf{Q}}{\partial t} + \frac{\partial}{\partial x}\mathbf{f}(\mathbf{Q}) = 0. \tag{21}$$

For this equation a classical conservative finite volume discretization, see e.g. [45,35], reads:

$$\mathbf{Q}_i^{n+1} = \mathbf{Q}_i^n - \frac{\Delta t}{\Delta x}\left(\mathbf{f}_{i+\frac{1}{2}} - \mathbf{f}_{i-\frac{1}{2}}\right), \tag{22}$$

using an equidistant grid with mesh spacing $\Delta x = x_{i+\frac{1}{2}} - x_{i-\frac{1}{2}}$ and a time step size of $\Delta t = t^{n+1} - t^n$. Here $\mathbf{Q}_i^n$ describes the usual cell average

$$\mathbf{Q}_i^n = \frac{1}{\Delta x}\int_{x_{i-\frac{1}{2}}}^{x_{i+\frac{1}{2}}} \mathbf{Q}(x, t^n)\, dx \tag{23}$$

at time t^n in cell number i and $\mathbf{f}_{i+\frac{1}{2}}$ is the numerical flux between the cells i and $i+1$. The numerical flux of the DOT Riemann solver [22] is then written as

$$\mathbf{f}_{i+\frac{1}{2}} = \frac{1}{2}\left(\mathbf{f}(\mathbf{Q}^+_{i+\frac{1}{2}}) + \mathbf{f}(\mathbf{Q}^-_{i+\frac{1}{2}})\right) - \frac{1}{2}\int_0^1 \left|\mathbf{A}\left(\Psi(\mathbf{Q}^-_{i+\frac{1}{2}}, \mathbf{Q}^+_{i+\frac{1}{2}}, s)\right)\right| \frac{\partial \Psi}{\partial s} ds, \tag{24}$$

where $\mathbf{Q}^+_{i+\frac{1}{2}}$ and $\mathbf{Q}^-_{i+\frac{1}{2}}$ are the boundary-extrapolated values at the interface and which are computed via a suitable nonlinear TVD reconstruction with appropriate slope limiters, see [45]. In our case, we simply use

$$\Delta \mathbf{Q}_i^n = \text{minmod}\left(\mathbf{Q}_i^n - \mathbf{Q}_{i-1}^n, \mathbf{Q}_{i+1}^n - \mathbf{Q}_i^n\right), \tag{25}$$

with the classical minmod slope limiter. The temporal evolution of the piecewise linear reconstruction polynomials is approximated by a discrete form of (21) as

$$\partial_t \mathbf{Q}_i^n = -\frac{\mathbf{f}(\mathbf{Q}_i^n + \frac{1}{2}\Delta \mathbf{Q}_i^n) - \mathbf{f}(\mathbf{Q}_i^n - \frac{1}{2}\Delta \mathbf{Q}_i^n)}{\Delta x}, \tag{26}$$

so that the boundary-extrapolated values within cell number i are given by

$$\mathbf{Q}^-_{i+\frac{1}{2}} = \mathbf{Q}_i^n + \frac{1}{2}\Delta \mathbf{Q}_i^n + \frac{1}{2}\Delta t \partial_t \mathbf{Q}_i^n, \qquad \text{and} \qquad \mathbf{Q}^+_{i-\frac{1}{2}} = \mathbf{Q}_i^n - \frac{1}{2}\Delta \mathbf{Q}_i^n + \frac{1}{2}\Delta t \partial_t \mathbf{Q}_i^n. \tag{27}$$

The symbol $\Psi(\mathbf{Q}^-_{i+\frac{1}{2}}, \mathbf{Q}^+_{i+\frac{1}{2}}, s)$ with $0 \le s \le 1$ is a path connecting the left state $\mathbf{Q}^-_{i+\frac{1}{2}}$ with the right state $\mathbf{Q}^+_{i+\frac{1}{2}}$ in phase-space, for which we have $\Psi(\mathbf{Q}^-_{i+\frac{1}{2}}, \mathbf{Q}^+_{i+\frac{1}{2}}, 0) = \mathbf{Q}^-_{i+\frac{1}{2}}$ and $\Psi(\mathbf{Q}^-_{i+\frac{1}{2}}, \mathbf{Q}^+_{i+\frac{1}{2}}, 1) = \mathbf{Q}^+_{i+\frac{1}{2}}$.

For the path we choose a simple straight line segment that connects the two states, i.e.

$$\Psi = \Psi(\mathbf{Q}^-_{i+\frac{1}{2}}, \mathbf{Q}^+_{i+\frac{1}{2}}, s) = \mathbf{Q}^-_{i+\frac{1}{2}} + s\left(\mathbf{Q}^+_{i+\frac{1}{2}} - \mathbf{Q}^-_{i+\frac{1}{2}}\right). \tag{28}$$

For a different choice of the path in the context of computational hemodynamics, see [39,40]. Since it is in general either not possible or very difficult to compute the integral in (24) analytically, the authors of [22] proposed to use a simple Gauss–Legendre quadrature rule. With these two simplifications we obtain for the numerical flux function of the DOT Riemann solver the following final expression:

$$\mathbf{f}_{i+\frac{1}{2}} = \frac{1}{2}\left(\mathbf{f}(\mathbf{Q}^+_{i+\frac{1}{2}}) + \mathbf{f}(\mathbf{Q}^-_{i+\frac{1}{2}})\right) - \frac{1}{2}\left(\sum_{j=1}^{N_G} \omega_j \left|\mathbf{A}\left(\Psi(s_j)\right)\right|\right)\left(\mathbf{Q}^+_{i+\frac{1}{2}} - \mathbf{Q}^-_{i+\frac{1}{2}}\right), \tag{29}$$

where $|\mathbf{A}| = \mathbf{R}|\mathbf{\Lambda}|\mathbf{R}^{-1}$ is the standard matrix absolute value operator with $|\mathbf{\Lambda}| = \text{diag}(|\lambda_1|, \ldots, |\lambda_i|, \ldots, |\lambda_m|)$. The weights ω_i and the nodes s_i are those of a standard Gauss–Legendre quadrature rule on the unit interval $[0, 1]$. For the numerical examples shown later, we use $N_G = 3$. Remember that in [9] Castro et al. have very recently proposed a cheap approximation of $|\mathbf{A}|$ inside the DOT Riemann solver by using the polynomial viscosity method of Degond et al. [16].

3.2. Review of the DOT Riemann solver for non-conservative hyperbolic systems

The DOT Riemann solver for non-conservative hyperbolic systems has been presented in [23]. In this case, one wants to discretize directly the quasi-linear form of the governing PDE (19) given by

$$\frac{\partial \mathbf{Q}}{\partial t} + \mathbf{A}(\mathbf{Q})\frac{\partial \mathbf{Q}}{\partial x} = 0. \tag{30}$$

A second order path-conservative finite volume scheme for such a system can be written according to Castro and Parés [43,10] as follows:

$$\mathbf{Q}_i^{n+1} = \mathbf{Q}_i^n - \frac{\Delta t}{\Delta x}\left(\mathbf{D}^-_{i+\frac{1}{2}} + \mathbf{D}^+_{i-\frac{1}{2}}\right) - \Delta t \mathbf{A}(\mathbf{Q}_i^{n+\frac{1}{2}})\frac{\Delta \mathbf{Q}_i^n}{\Delta x}, \tag{31}$$

with the slope $\Delta \mathbf{Q}_i^n$ computed according to (25). Furthermore, we have

$$\mathbf{Q}_i^{n+\frac{1}{2}} = \mathbf{Q}_i^n + \frac{1}{2}\Delta t \partial_t \mathbf{Q}_i^n, \qquad \text{and} \qquad \partial_t \mathbf{Q}_i^n = -\mathbf{A}(\mathbf{Q}_i^n)\frac{\Delta \mathbf{Q}_i^n}{\Delta x}. \tag{32}$$

The jump terms on the element boundaries must satisfy the following consistency condition:

$$\mathbf{D}^+_{i+\frac{1}{2}} + \mathbf{D}^-_{i+\frac{1}{2}} = \int_0^1 \mathbf{A}\left(\Psi(\mathbf{Q}^-_{i+\frac{1}{2}}, \mathbf{Q}^+_{i+\frac{1}{2}}, s)\right)\frac{\partial \Psi}{\partial s} ds. \tag{33}$$

In the case of the DOT Riemann solver [23] the jump terms read

$$\mathbf{D}^\pm_{i+\frac{1}{2}} = \frac{1}{2}\int_0^1 \left(\mathbf{A}\left(\Psi(\mathbf{Q}^-_{i+\frac{1}{2}}, \mathbf{Q}^+_{i+\frac{1}{2}}, s)\right) \pm \left|\mathbf{A}\left(\Psi(\mathbf{Q}^-_{i+\frac{1}{2}}, \mathbf{Q}^+_{i+\frac{1}{2}}, s)\right)\right|\right)\frac{\partial \Psi}{\partial s} ds. \tag{34}$$

For the straight-line segment path, this relation simplifies to

$$\mathbf{D}^\pm_{i+\frac{1}{2}} = \frac{1}{2}\left(\int_0^1 \left(\mathbf{A}\left(\Psi(\mathbf{Q}^-_{i+\frac{1}{2}}, \mathbf{Q}^+_{i+\frac{1}{2}}, s)\right) \pm \left|\mathbf{A}\left(\Psi(\mathbf{Q}^-_{i+\frac{1}{2}}, \mathbf{Q}^+_{i+\frac{1}{2}}, s)\right)\right|\right) ds\right)\left(\mathbf{Q}^+_{i+\frac{1}{2}} - \mathbf{Q}^-_{i+\frac{1}{2}}\right), \tag{35}$$

where the path integral is subsequently approximated by a Gaussian quadrature formula in the same way as described in the previous section:

$$\mathbf{D}^\pm_{i+\frac{1}{2}} = \frac{1}{2}\left(\sum_{j=1}^{N_G} \omega_j \left(\mathbf{A}\left(\Psi(\mathbf{Q}^-_{i+\frac{1}{2}}, \mathbf{Q}^+_{i+\frac{1}{2}}, s_j)\right) \pm \left|\mathbf{A}\left(\Psi(\mathbf{Q}^-_{i+\frac{1}{2}}, \mathbf{Q}^+_{i+\frac{1}{2}}, s_j)\right)\right|\right)\right)\left(\mathbf{Q}^+_{i+\frac{1}{2}} - \mathbf{Q}^-_{i+\frac{1}{2}}\right). \tag{36}$$

3.3. The DOT Riemann solver for the combined system

The two solvers that have been briefly summarized in the two previous sections are now applied to solve the full combined system (19). After proper rearrangement of terms and making use of the consistency condition (33), we can write the following explicit second order TVD finite volume scheme for (19):

$$\mathbf{Q}_i^{n+1} = \mathbf{Q}_i^n - \frac{\Delta t}{\Delta x}\left(\mathbf{f}_{i+\frac{1}{2}} - \mathbf{f}_{i-\frac{1}{2}}\right) - \frac{\Delta t}{\Delta x}\left(\mathbf{D}_{i+\frac{1}{2}} + \mathbf{D}_{i-\frac{1}{2}}\right) - \Delta t \mathbf{B}(\mathbf{Q}_i^{n+\frac{1}{2}})\frac{\Delta \mathbf{Q}_i^n}{\Delta x} + \Delta t \mathbf{S}(\mathbf{Q}_i^{n+\frac{1}{2}}). \tag{37}$$

The slopes $\Delta \mathbf{Q}_i^n$ are again computed from (25), while the time derivative is now approximated by a discrete version of the entire system (19) as

$$\partial_t \mathbf{Q}_i^n = -\frac{\mathbf{f}(\mathbf{Q}_i^n + \frac{1}{2}\Delta \mathbf{Q}_i^n) - \mathbf{f}(\mathbf{Q}_i^n - \frac{1}{2}\Delta \mathbf{Q}_i^n)}{\Delta x} - \mathbf{B}(\mathbf{Q}_i^n)\frac{\Delta \mathbf{Q}_i^n}{\Delta x} + \mathbf{S}(\mathbf{Q}_i^n). \tag{38}$$

We still have the relation $\mathbf{Q}_i^{n+\frac{1}{2}} = \mathbf{Q}_i^n + \frac{1}{2}\Delta t \partial_t \mathbf{Q}_i^n$. The numerical flux of the DOT solver in the scheme for the combined system (37) is defined as

$$\mathbf{f}_{i+\frac{1}{2}} = \frac{1}{2}\left(\mathbf{f}(\mathbf{Q}^+_{i+\frac{1}{2}}) + \mathbf{f}(\mathbf{Q}^-_{i+\frac{1}{2}})\right) - \frac{1}{2}\int_0^1 \left|\mathbf{A}\left(\Psi(\mathbf{Q}^-_{i+\frac{1}{2}}, \mathbf{Q}^+_{i+\frac{1}{2}}, s)\right)\right|\frac{\partial \Psi}{\partial s} ds, \tag{39}$$

hence it contains a numerical dissipation based on the system matrix $\mathbf{A}$ that includes both, conservative and non-conservative terms. The non-conservative jump terms then simply read

$$\mathbf{D}_{i+\frac{1}{2}} = \frac{1}{2}\int_0^1 \mathbf{B}\left(\Psi(\mathbf{Q}^-_{i+\frac{1}{2}}, \mathbf{Q}^+_{i+\frac{1}{2}}, s)\right)\frac{\partial \Psi}{\partial s} ds. \tag{40}$$

Approximating the above relations with a Gauss–Legendre quadrature formula, we get the final expressions for the numerical flux and the jump terms in (37):

$$\mathbf{f}_{i+\frac{1}{2}} = \frac{1}{2}\left(\mathbf{f}(\mathbf{Q}^+_{i+\frac{1}{2}}) + \mathbf{f}(\mathbf{Q}^-_{i+\frac{1}{2}})\right) - \frac{1}{2}\left(\sum_{j=1}^{N_G} \omega_j \left|\mathbf{A}\left(\Psi(\mathbf{Q}^-_{i+\frac{1}{2}}, \mathbf{Q}^+_{i+\frac{1}{2}}, s_j)\right)\right|\right)\left(\mathbf{Q}^+_{i+\frac{1}{2}} - \mathbf{Q}^-_{i+\frac{1}{2}}\right), \tag{41}$$

and

$$\mathbf{D}_{i+\frac{1}{2}} = \frac{1}{2}\left(\sum_{j=1}^{N_G} \omega_j \mathbf{B}\left(\Psi(\mathbf{Q}^-_{i+\frac{1}{2}}, \mathbf{Q}^+_{i+\frac{1}{2}}, s_j)\right)\right)\left(\mathbf{Q}^+_{i+\frac{1}{2}} - \mathbf{Q}^-_{i+\frac{1}{2}}\right). \tag{42}$$

3.4. Eigenstructure of the governing PDE needed by the DOT Riemann solver

We now want to solve the particular system of governing equations (10)–(13) for the compressible flow in compliant visco-elastic tubes, as described in Section 2.3. Since the system can be cast into the general form (19), the path-conservative finite volume scheme (37) based on the DOT Riemann solver is used. For the evaluation of the matrix absolute value operator $|\mathbf{A}|$, we need to know all the eigenvalues and the eigenvectors of the governing PDE system. In particular, we have:

$$\mathbf{Q} = \begin{pmatrix} A\rho \\ A\rho u \\ A \\ A_0 \end{pmatrix} = \begin{pmatrix} Q_1 \\ Q_2 \\ Q_3 \\ Q_4 \end{pmatrix}, \qquad \mathbf{f}(\mathbf{Q}) = \begin{pmatrix} A\rho u \\ A\rho u^2 + Ap \\ 0 \\ 0 \end{pmatrix}, \qquad \mathbf{B} = \begin{pmatrix} 0 & 0 & 0 & 0 \\ 0 & 0 & -p & 0 \\ 0 & d & 0 & 0 \\ 0 & 0 & 0 & 0 \end{pmatrix}. \tag{43}$$

With $p = p(\rho) = p(Q_1/Q_3)$, the Jacobian of the flux and the complete system matrix $\mathbf{A}(\mathbf{Q})$ read

$$\frac{\partial \mathbf{f}}{\partial \mathbf{Q}} = \begin{pmatrix} 0 & 1 & 0 & 0 \\ -u^2 + a & 2u & p + b & 0 \\ 0 & 0 & 0 & 0 \\ 0 & 0 & 0 & 0 \end{pmatrix}, \qquad \mathbf{A}(\mathbf{Q}) = \frac{\partial \mathbf{f}}{\partial \mathbf{Q}} + \mathbf{B}(\mathbf{Q}) = \begin{pmatrix} 0 & 1 & 0 & 0 \\ -u^2 + a & 2u & b & 0 \\ 0 & d & 0 & 0 \\ 0 & 0 & 0 & 0 \end{pmatrix}, \tag{44}$$

with $a = Q_3 \frac{\partial p}{\partial Q_1} = c^2$ and $b = Q_3 \frac{\partial p}{\partial Q_3} = -\rho c^2$. The eigenvalue decomposition of $\mathbf{A}(\mathbf{Q}) = \mathbf{R}\mathbf{\Lambda}\mathbf{R}^{-1}$ is:

$$\mathbf{\Lambda} = \begin{pmatrix} 0 & 0 & 0 & 0 \\ 0 & 0 & 0 & 0 \\ 0 & 0 & u - \sqrt{a + bd} & 0 \\ 0 & 0 & 0 & u + \sqrt{a + bd} \end{pmatrix}, \qquad \mathbf{R} = \begin{pmatrix} -\frac{b}{a-u^2} & 0 & \frac{1}{d} & \frac{1}{d} \\ 0 & 0 & \frac{u-\sqrt{a+bd}}{d} & \frac{u+\sqrt{a+bd}}{d} \\ 1 & 0 & 1 & 1 \\ 0 & 1 & 0 & 0 \end{pmatrix}, \tag{45}$$

$$\mathbf{R}^{-1} = \frac{1}{\sqrt{a + bd}} \begin{pmatrix} -\frac{d\,(a-u^2)\sqrt{a+bd}}{-u^2+a+bd} & 0 & \frac{(a-u^2)\sqrt{a+bd}}{-u^2+a+bd} & 0 \\ 0 & 0 & 0 & \sqrt{a+bd} \\ \frac{d\,(u+\sqrt{a+bd})\,(a-u^2)}{2(-u^2+a+bd)} & -\frac{d}{2} & \frac{bd\,(u+\sqrt{a+bd})}{2(-u^2+a+bd)} & 0 \\ -\frac{d\,(u-\sqrt{a+bd})\,(a-u^2)}{2(-u^2+a+bd)} & \frac{d}{2} & -\frac{bd\,(u-\sqrt{a+bd})}{2(-u^2+a+bd} & 0 \end{pmatrix}. \tag{46}$$

For hyperbolicity of the system (19), the term $a + bd$ needs to be positive. For the law of Laplace we have:

$$\begin{aligned} & a + bd > 0 \\ c^2 + (-\rho c^2)\frac{1}{\frac{\beta A}{c^2} + \rho} > 0, \qquad & \text{with } c^2,\ \rho,\ A,\ \beta > 0 \\ 1 > \rho \frac{1}{\frac{\beta A}{c^2} + \rho} & \\ \frac{\beta A}{\rho c^2} + 1 > 1 & \\ \frac{\beta A}{\rho c^2} > 0, \qquad & \text{which is always true.} \end{aligned}$$

And for the Maxwell model:

$$\begin{aligned} & a + bd > 0 \\ c^2 + (-\rho c^2)\frac{1}{\frac{E_0 \phi}{2Wc^2} + \rho} > 0, \qquad & \text{with } c^2, \rho, \phi, E_0, W\ > 0 \end{aligned}$$

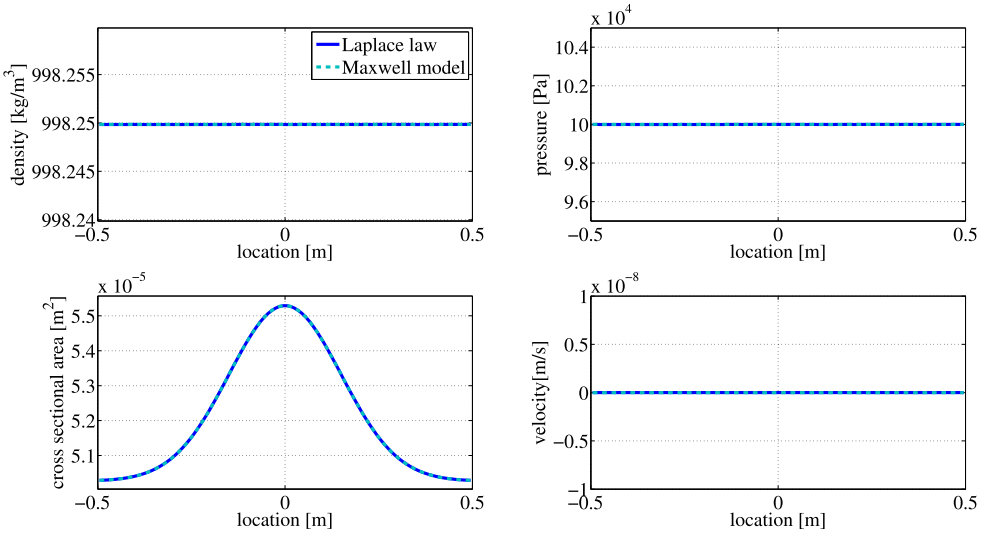

Fig. 2. Test of the well-balanced property. Results for the steady state solution with a smooth reference cross section A_0 for the two material models at time $t = 4 \cdot 10^{-3}$.

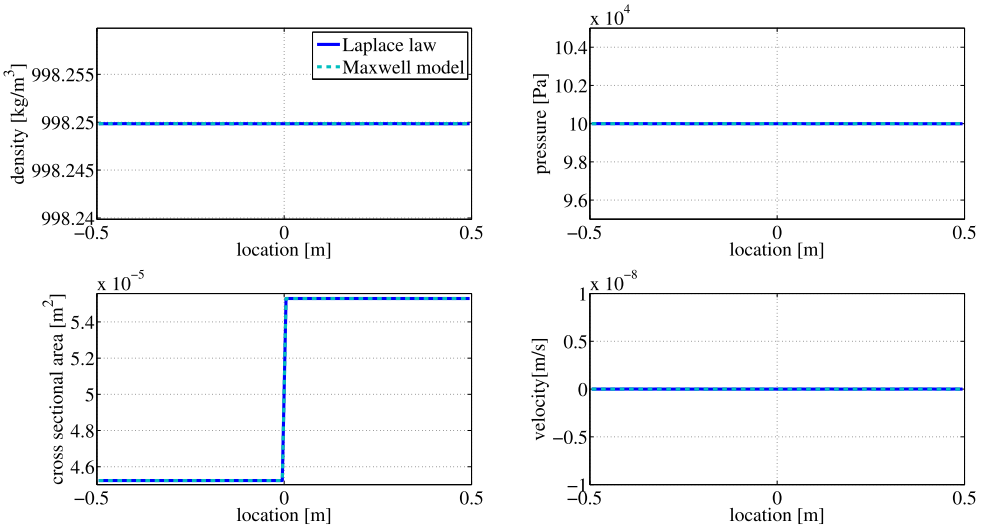

Fig. 3. Test of the well-balanced property. Results for the steady state solution with a discontinuous reference cross section A_0 for the two material models at time $t = 4 \cdot 10^{-3}$.

$$1 > \rho \frac{1}{\frac{E_0 \phi}{2Wc^2} + \rho}$$

$$\frac{E_0 \phi}{2Wc^2 \rho} + 1 > 1$$

$$\frac{E_0 \phi}{2Wc^2 \rho} > 0, \qquad \text{which is always true.}$$

4. Numerical results

For the numerical verification of the finite volume scheme (37) with the DOT Riemann solver, we run two different types of test problems. First, we solve a set of Riemann problems for the Laplace law, for which a quasi-exact reference solution has been derived in [20], and for the Maxwell model, where a fine-grid reference solution is provided. To show the correctness of the model for the material of the tube wall, we compare the results obtained from the numerical simulation of a time-harmonic wave traveling in an elastic tube with analytical results obtained in the frequency domain and with experimental data available for a polymer tube. The CFL number used in all simulations shown in this paper was CFL = 0.9.

Table 1
Initial states for Riemann problems $(p[Pa], u[m/s])$.

Case	p_L	u_L	p_R	u_R	β	Number of cells
RP1	10^6	0	10^5	0	$4 \cdot 10^{32}$	200
RP2	10^6	0	10^5	0	$4 \cdot 10^{13}$	200
RP3	10^5	-1	10^5	$+1$	$4 \cdot 10^{32}$	500
RP4	10^5	-1	10^5	$+1$	$4 \cdot 10^{13}$	500
RP5	10^3	0	10^2	0	$4 \cdot 10^{32}$	500
RP6	10^5	0	10^2	0	$4 \cdot 10^{13}$	500

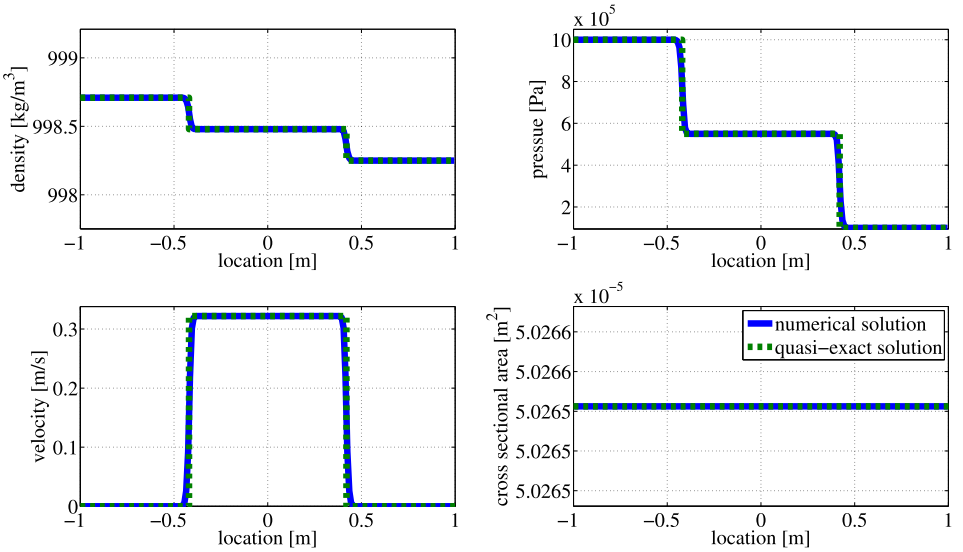

Fig. 4. Comparison of the numerical results obtained with the path-conservative finite volume scheme and the DOT Riemann solver to the quasi-exact solution for RP1 at time $t = 3 \cdot 10^{-4}$.

4.1. Well-balancing

The governing PDE system (10)–(13) admits a particular steady state solution that reads

$$\rho = const., \qquad u = 0, \qquad A = A_0, \qquad A_0 > 0, \tag{47}$$

where A_0 is an arbitrary positive function. This condition is similar to the steady lake at rest solution of the shallow water equations, and requires special care in the design of the numerical scheme, see [34,30,28,29,3,26,1,10,43,25,8,12,39,17], for example. In this section, we test the well-balanced property (the so-called C-property) of our DOT Riemann solver numerically by solving the following test problem. We consider a tube $\Omega = [-L/2, +L/2]$ of length L, the initial condition for the density, the velocity and the cross sectional area are given by $\rho = \rho_0$, $u = 0$ and $A = A_0$, respectively, while the reference cross section A_0 at equilibrium has the following profile:

$$A_0(x) = \bar{A} + \delta A \exp\left(-\frac{1}{2}\frac{x^2}{\sigma^2}\right), \qquad \text{(smooth test case)}, \tag{48}$$

$$A_0(x) = \frac{1}{2}\left(1 - \text{sign}(x)\right)\bar{A}_L + \frac{1}{2}\left(1 + \text{sign}(x)\right)\bar{A}_R, \qquad \text{(discontinuous test case)}. \tag{49}$$

For the parameters of this test case we choose $\rho_0 = 998.2498$, $p_{ext} = 10^5$, $L = 1$, $\bar{A} = 5.0265 \cdot 10^{-5}$, $\delta A = 5.0265 \cdot 10^{-6}$, $\sigma = 0.15$, $\bar{A}_L = 4.5239 \cdot 10^{-5}$ and $\bar{A}_R = 5.5292 \cdot 10^{-5}$, respectively. The final simulation time is chosen as $t = 4 \cdot 10^{-3}$ and the computational results obtained on a mesh composed of 100 equidistant grid points are plotted in Figs. 2 and 3. The observed L_∞ error of the velocity u with respect to the exact solution ($u = 0$) was $8.9636 \cdot 10^{-13}$ with the Laplace law and 0.0 with the Maxwell model for the smooth test case. For the discontinuous test case, the L_∞ error of the velocity u was $1.9184 \cdot 10^{-12}$ with the Laplace law and 0.0 with the Maxwell model. These numerical results clearly confirm that the presented approach is *well-balanced*, which was expected, thanks to the use of a path-conservative finite volume scheme. At this point we would like to emphasize that the family of path-conservative methods proposed by Parés and Castro and co-workers in [10,43,25,8,12,39] provides a very nice and *direct* way for constructing *naturally well-balanced* Godunov-type finite volume schemes for hyperbolic PDE with non-conservative products, even for rather complex PDE systems like the system solved in [39], or the model (10)–(13) used in this paper.

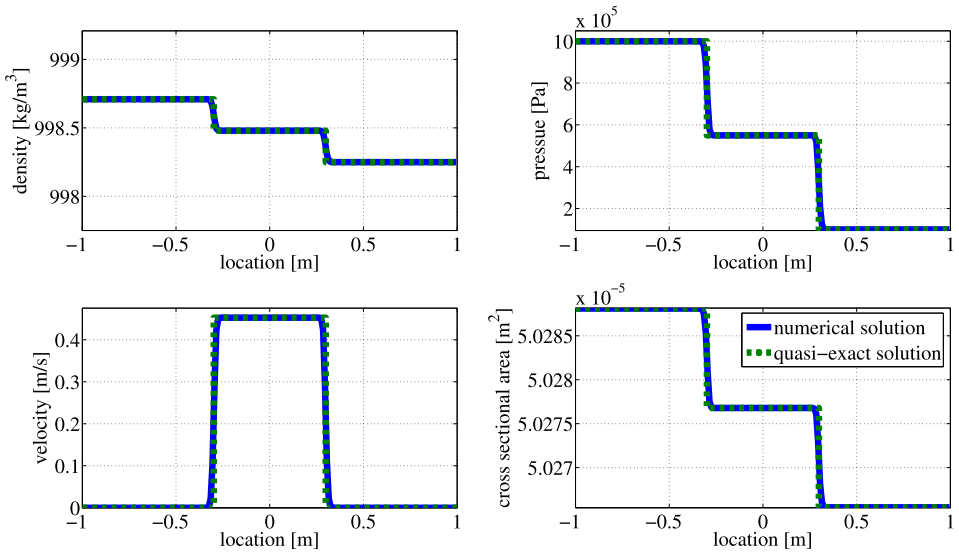

Fig. 5. Comparison of the numerical results obtained with the path-conservative finite volume scheme and the DOT Riemann solver to the quasi-exact solution for RP2 at time $t = 3 \cdot 10^{-4}$.

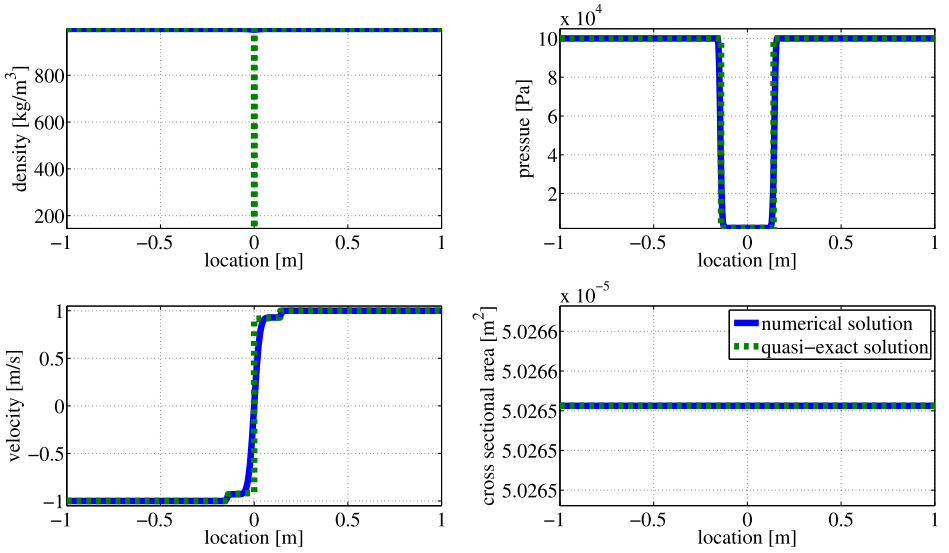

Fig. 6. Comparison of the numerical results obtained with the path-conservative finite volume scheme and the DOT Riemann solver to the quasi-exact solution for RP3 at time $t = 1 \cdot 10^{-4}$.

4.2. Riemann problems

The initial conditions of the following Riemann problems are summarized in Table 1. First, we solve them applying the Laplace law and comparing the results to the quasi-exact solution provided in [20]. Then, some of the problems are solved again with the Maxwell model, but because of the time dependence of the material it is not possible to compare it to the quasi-exact solution. RP1 consists of a flow in a rigid tube, where the fluid remains liquid. RP 2 is similar to RP1, but with a flexible tube. The Riemann problems RP3 and RP5 consider the flow in a rigid pipe, where the fluid consists of a mixture of liquid and vapor. RP4 and RP6 are similar to RP3 and RP5, but for a flexible tube.

4.2.1. Riemann problems for the Laplace law

For the Laplace law the numerical solution is compared to a quasi-exact solution of RP1–RP6 (see [20]). For a thorough discussion of the exact solution of the Riemann problem of the 1D Euler equations in a rigid duct with spatially variable cross section, see [31] and [44], where in the latter reference also a very detailed comparison with fully three-dimensional simulations has been provided. For a quasi-exact Riemann solver of the Euler equations with general equation of state, see

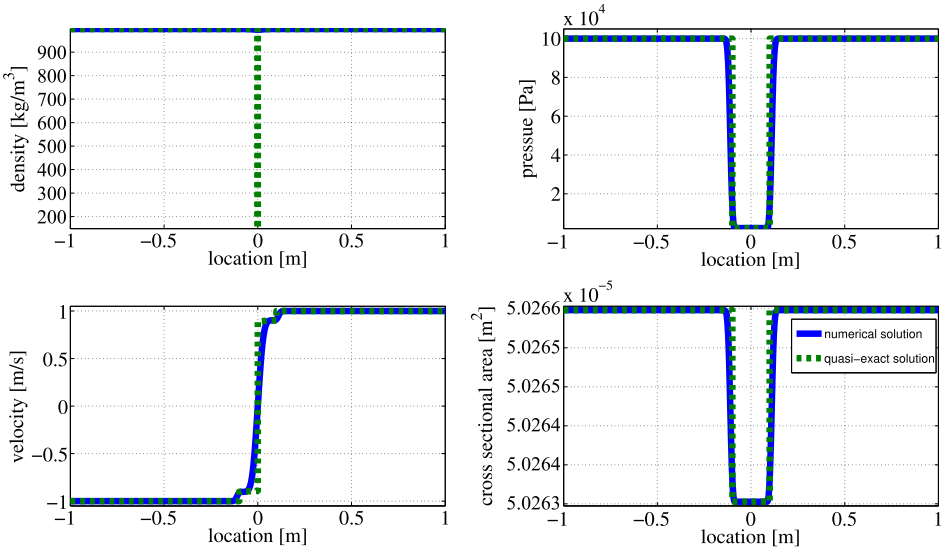

Fig. 7. Comparison of the numerical results obtained with the path-conservative finite volume scheme and the DOT Riemann solver to the quasi-exact solution for RP4 at time $t = 1 \cdot 10^{-4}$.

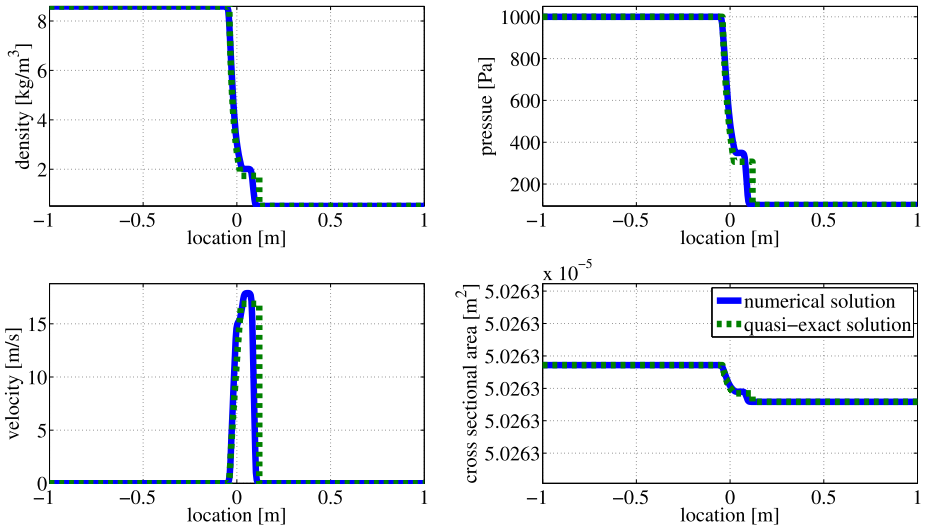

Fig. 8. Comparison of the numerical results obtained with the path-conservative finite volume scheme and the DOT Riemann solver to the quasi-exact solution for RP5 at time $t = 5 \cdot 10^{-3}$.

[21], for example. The results of this calculations for the different RP are shown in Figs. 4–9. One can observe that for most of the Riemann problems, the agreement between the exact solution and the numerical solution is good.

4.2.2. Riemann problems for the Maxwell model

We now solve some of the Riemann problems listed in Table 1, but using this time the Maxwell model for the tube wall. The parameters for calculating the Riemann problems with the Maxwell model are $E_\infty = 8 \cdot 10^8$, $E_0 = 10^8$ and $\eta = 10^4$. In Fig. 10 we compare the numerical solution of RP2 on a coarse gird (100 cells) to a numerical solution on a very fine grid (5000 cells). In Figs. 11, 12 and 13 the time evolution of the variables is presented along the tube axis at different intermediate output times. One can see that with increasing time, the tube is reaching an equilibrium state. Compared to the solution of RP2 for the Laplace law (Fig. 5), one can recognize the time depended relaxation of the model. While in the plot for the cross sectional area for the Laplace law the change between the different stages of strain is quite sharp, it is a lot smoother for the Maxwell model, which is a direct result of the visco-elastic material behavior.

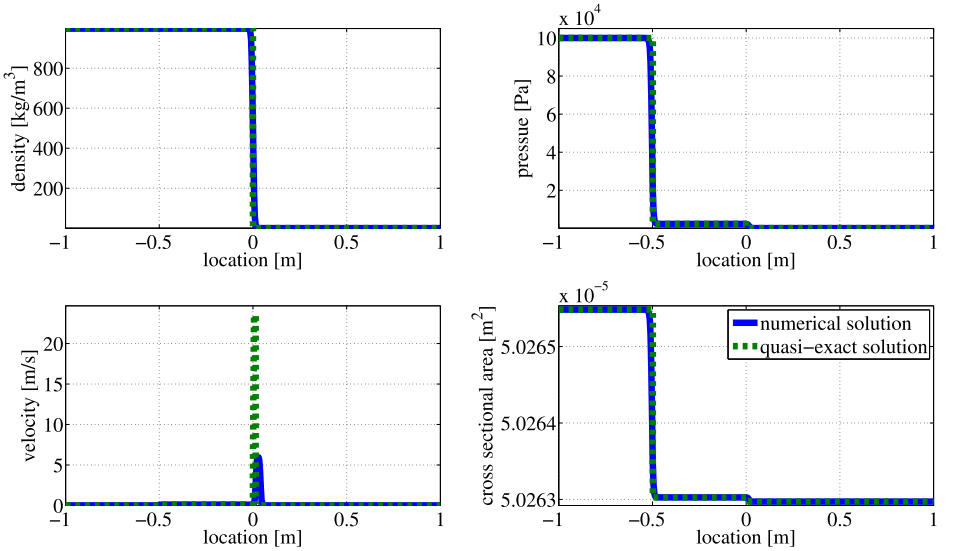

Fig. 9. Comparison of the numerical results obtained with the path-conservative finite volume scheme and the DOT Riemann solver to the quasi-exact solution for RP6 at time $t = 5 \cdot 10^{-4}$.

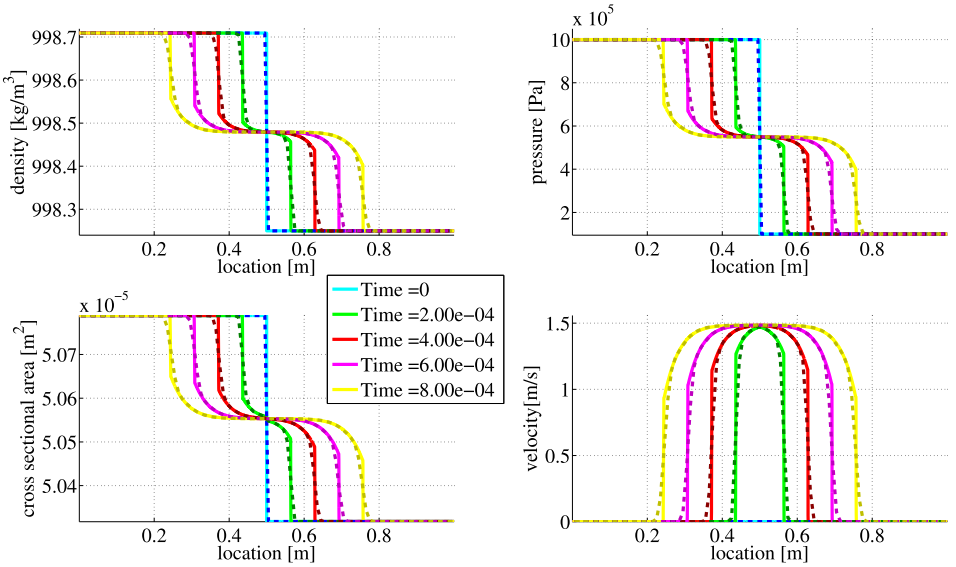

Fig. 10. Time evolution of RP2 with Maxwell model on a coarse grid (dashed line) compared to a reference solution obtained on a very fine grid (solid line)

4.3. Comparison with experimental results

For the correct understanding of complex hydraulic systems it is necessary to simulate the dynamic behavior of the flexible tubes used in such systems accurately. In Fig. 16(a) one can see an example of a homogeneous flexible tube that is typically used in industrial hydraulic systems. To be sure that the numerical model can reproduce the dynamic behavior of such a tube, we validate our results with analytical results obtained in the frequency domain and with available experimental data.

The experimental system is roughly depicted in Fig. 14. There, one can see that the test object is excited on the boundaries by a sinusoidal pressure wave with a fixed frequency. This excitation is done for frequencies between 0 and 2000 Hz. During the experiment the pressure and the volumetric flow rate are indirectly measured at the in- and outlet of the test object. Using the transfer matrix method for linear dynamic systems, one can get the dynamic performance of the tube at each frequency. A detailed description of the experimental set-up and the computation of the exact solution in the frequency domain is shown in the work of Leonhardt, [33], who also kindly provided the experimental measurements.

In Fig. 15 one can see the comparison of the numerical results with the experimental ones for a homogeneous polymer tube. In the graphs, the ratio of the pressure at the outlet and the inlet (p_2/p_1) of the tube over the frequencies is shown.

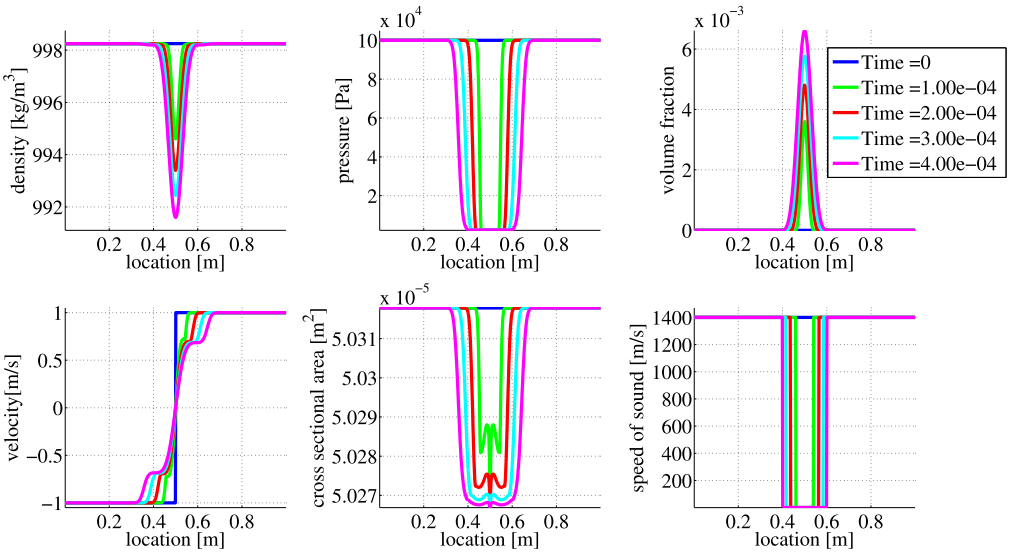

Fig. 11. Time evolution of RP4 with Maxwell model for the tube wall.

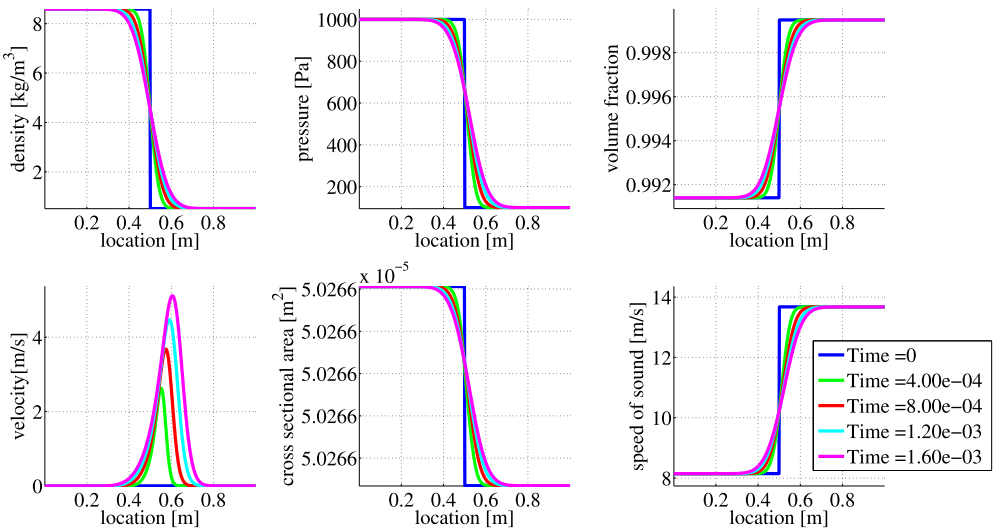

Fig. 12. Time evolution of RP5 with Maxwell model for the tube wall.

When the friction effect is neglected in our calculations, there is a visible disagreement compared to the experimental results. But when comparing the results of the numerical simulation to the exact solution obtained in the frequency domain without friction, the agreement is excellent. When we add friction to the quasi-exact solution in the frequency domain and to our time-domain simulations based on the path-conservative finite volume scheme, we can reproduce the results from the experiment reasonably well for frequencies up to 800 Hz. As friction model, we use the frequency-dependent friction model proposed by Zielke, see [47] and [33]. In the time domain, a suitable approximation for the Zielke model is used. There are two different reasons for the visible discrepancy between simulation and experiment beyond 800 Hz. First, the experimental data are less reliable for higher frequencies, which can also be seen in the unphysical jumps present in the experimental results beyond 1000 Hz, which are clearly visible in Fig. 15. Second, to obtain a better match of the numerical simulations with the experimental data, one would need either a more complex multi-parameter Maxwell model, consisting of several spring-dashpot combinations, or even a full PDE model for the visco-elastic wall that also accounts for momentum transfer inside the wall in axial direction.

5. Conclusion

In this paper we presented a system of PDE that represents the fluid–structure interaction for a compressible fluid flowing in a flexible visco-elastic tube. A 3-parameter Maxwell model has been used to represent the time dependent

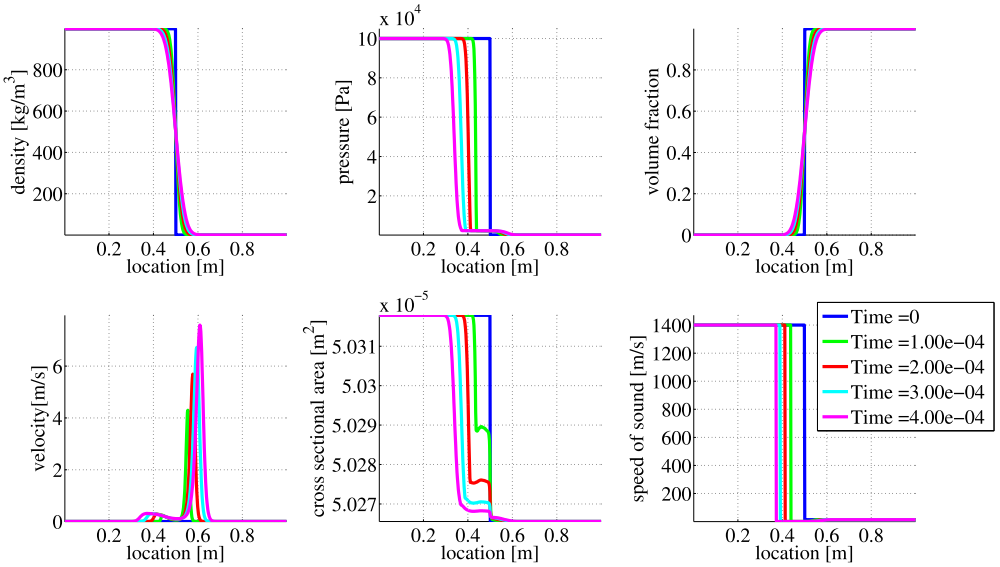

Fig. 13. Time evolution of RP6 with Maxwell model for the tube wall.

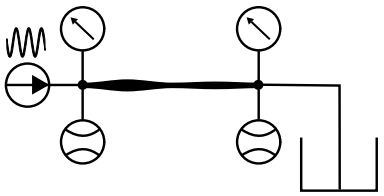

Fig. 14. Experimental set-up to measure the dynamic performance of a tube

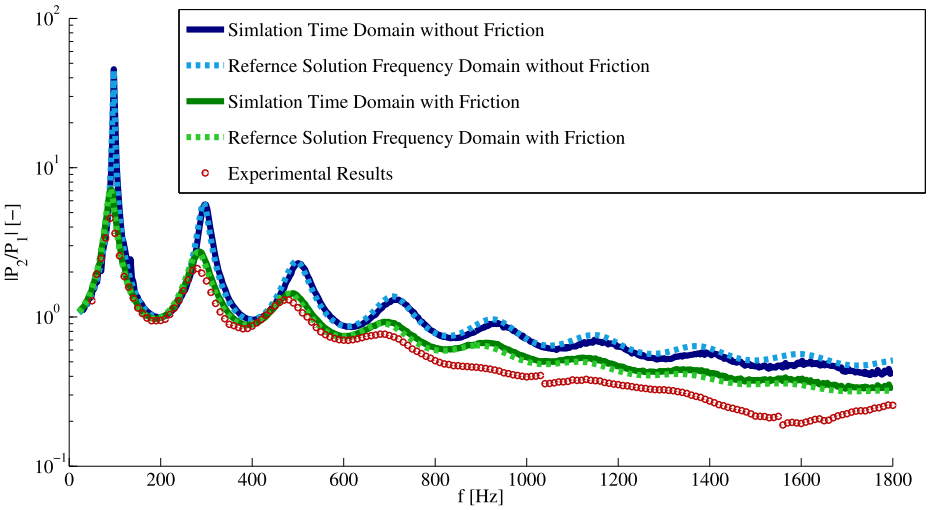

Fig. 15. Comparison of the time-domain simulation with the path-conservative finite volume scheme to an exact solution in the frequency domain and to experimental results, both of which have been very kindly provided by R. Leonhardt [33].

relaxation of the polymer material of the tube wall. For the fluid flow the cross-sectionally averaged Euler equations have been used. The fluid was modeled by a barotropic equation of state that includes also a simple cavitation model. The coupled equation system was then solved by a path-conservative finite volume scheme based on a generalization of the Riemann solver of Osher and Solomon proposed by Dumbser and Toro in [23,22] (DOT Riemann solver). The proposed scheme can handle hyperbolic PDE with a conservative and a non-conservative part. With these mathematical models and

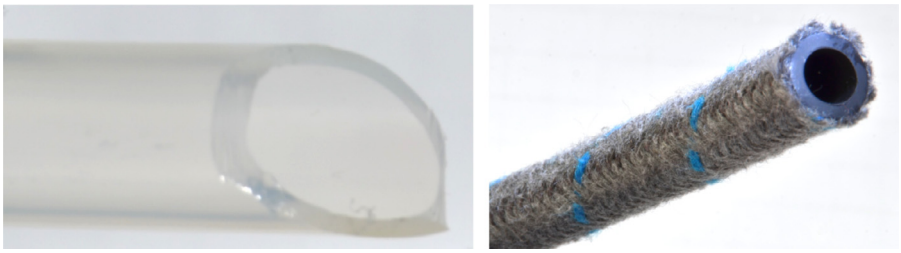

(a) Homogeneous polymer tube (b) A complex flexible tube with two layers

Fig. 16. Different types of flexible tubes.

the path-conservative finite volume scheme based on the DOT Riemann solver we were able to reproduce the dynamic behavior of a flexible polymer tube used in industrial hydraulic systems.

As future work the model of the tube wall will be extended, so that we will be also able to reproduce the dynamic behavior of a more complex flexible tube. That means that we will model for example a tube composed of two layers, as depicted in Fig. 16(b). For this 1D model we want to identify at first the most relevant physical effects, for which we will then derive a suitable set of governing PDE. Finally, a new efficient numerical method will be designed for this more complex PDE system.

Acknowledgements

The research presented in this paper was financially supported by the Robert Bosch GmbH, Germany. The authors are very grateful to R. Leonhardt for the very inspiring discussions on the topic and for kindly providing the exact solution in the frequency-domain as well as the experimental data for the time-harmonic excitation of a visco-elastic polymer tube.

The authors are very grateful for the constructive comments and remarks provided by the two referees of this manuscript.

References

[1] E. Audusse, F. Bouchut, M. Bristeau, R. Klein, B. Perthame, A fast and stable well-balanced scheme with hydrostatic reconstruction for shallow water flows, SIAM J. Sci. Comput. 25 (2004) 2050–2065.
[2] O.A. Bauchau, J.I. Craig, Structural Analysis, Springer, 2009.
[3] A. Bermúdez, M.E. Vázquez-Cendón, Upwind methods for hyperbolic conservation laws with source terms, Comput. Fluids 23 (1994) 1049–1071.
[4] L. Brugnano, V. Casulli, Iterative solution of piecewise linear systems, SIAM J. Sci. Comput. 30 (2007) 463–472.
[5] L. Brugnano, V. Casulli, Iterative solution of piecewise linear systems and applications to flows in porous media, SIAM J. Sci. Comput. 31 (2009) 1858–1873.
[6] L. Brugnano, A. Sestini, Iterative solution of piecewise linear systems for the numerical solution of obstacle problems, J. Numer. Anal. Ind. Appl. Math. 6 (2012) 67–82.
[7] M. Castro, E. Fernández, A. Ferriero, J. García, C. Parés, High order extensions of Roe schemes for two dimensional nonconservative hyperbolic systems, J. Sci. Comput. 39 (2009) 67–114.
[8] M. Castro, J. Gallardo, J. López, C. Parés, Well-balanced high order extensions of Godunov's method for semilinear balance laws, SIAM J. Numer. Anal. 46 (2008) 1012–1039.
[9] M. Castro, J. Gallardo, A. Marquina, Approximate Osher–Solomon schemes for hyperbolic systems, Appl. Math. Comput. 272 (2016) 347–368.
[10] M. Castro, J. Gallardo, C. Parés, High-order finite volume schemes based on reconstruction of states for solving hyperbolic systems with nonconservative products. applications to shallow-water systems, Math. Comput. 75 (2006) 1103–1134.
[11] M. Castro, P. LeFloch, M. Muñoz-Ruiz, C. Parés, Why many theories of shock waves are necessary: convergence error in formally path-consistent schemes, J. Comput. Phys. 227 (2008) 8107–8129.
[12] M. Castro, A. Pardo, C. Parés, E. Toro, On some fast well-balanced first order solvers for nonconservative systems, Math. Comput. 79 (2010) 1427–1472.
[13] V. Casulli, M. Dumbser, E.F. Toro, Semi-implicit numerical modeling of axially symmetric flows in compliant arterial systems, Int. J. Numer. Methods Biomed. Eng. 28 (2012) 257–272.
[14] V. Casulli, P. Zanolli, A nested Newton-type algorithm for finite volume methods solving Richards' equation in mixed form, SIAM J. Sci. Comput. 32 (2009) 2255–2273.
[15] V. Casulli, P. Zanolli, Iterative solutions of mildly nonlinear systems, J. Comput. Appl. Math. 236 (2012) 3937–3947.
[16] P. Degond, P. Peyrard, G. Russo, P. Villedieu, Polynomial upwind schemes for hyperbolic systems, C. R. Acad. Sci., Ser. 1 Math. 328 (1999) 479–483.
[17] M. Dumbser, D. Balsara, A new efficient formulation of the HLLEM Riemann solver for general conservative and non-conservative hyperbolic systems, J. Comput. Phys. 304 (2016) 275–319.
[18] M. Dumbser, M. Castro, C. Parés, E.F. Toro, Ader schemes on unstructured meshes for nonconservative hyperbolic systems: applications to geophysical flows, Comput. Fluids 38 (2009) 1731–1748.
[19] M. Dumbser, A. Hidalgo, M. Castro, C. Parés, E.F. Toro, Force schemes on unstructured meshes ii: non-conservative hyperbolic systems, Comput. Methods Appl. Mech. Eng. 199 (2010) 625–647.
[20] M. Dumbser, U. Iben, M. Ioriatti, An efficient semi-implicit finite volume method for axially symmetric compressible flows in compliant tubes, Appl. Numer. Math. 89 (2015) 24–44.
[21] M. Dumbser, U. Iben, C.D. Munz, Efficient implementation of high order unstructured WENO schemes for cavitating flows, Comput. Fluids 86 (2013) 141–168.
[22] M. Dumbser, E.F. Toro, On universal Osher–type schemes for general nonlinear hyperbolic conservation laws, Commun. Comput. Phys. 10 (2011) 635–671.

[23] M. Dumbser, E.F. Toro, A simple extension of the Osher Riemann solver to non-conservative hyperbolic systems, J. Sci. Comput. 48 (2011) 70–88.
[24] R. Etlender, Modellierung und Simulation der Wellenausbreitung in flexiblen hydraulischen Leitungen, Ph.D. thesis, Universität Stuttgart, 2012.
[25] J. Gallardo, C. Parés, M. Castro, On a well-balanced high-order finite volume scheme for shallow water equations with topography and dry areas, J. Comput. Phys. 227 (2007) 574–601.
[26] P. Garcia-Navarro, M. Vázquez-Cendón, On numerical treatment of the source terms in the shallow water equations, Comput. Fluids 29 (2000) 951–979.
[27] M. Goeke, Modellierung der Materialdämpfung bei der Wellenausbreitung in flexiblen Leitungen, Master's thesis, University Stuttgart, 2013.
[28] L. Gosse, A well-balanced flux-vector splitting scheme designed for hyperbolic systems of conservation laws with source terms, Comput. Math. Appl. 39 (2000) 135–159.
[29] L. Gosse, A well-balanced scheme using non-conservative products designed for hyperbolic systems of conservation laws with source terms, Math. Models Methods Appl. Sci. 11 (2001) 339–365.
[30] J.M. Greenberg, A.Y.L. Roux, A wellbalanced scheme for the numerical processing of source terms in hyperbolic equations, SIAM J. Numer. Anal. 33 (1996) 1–16.
[31] E. Han, M. Hantke, G. Warnecke, Exact Riemann solutions to compressible Euler equations in ducts with discontinuous cross-section, J. Hyperbolic Differ. Equ. 9 (2012) 403–449.
[32] R. Lakes, Viscoelastic Solids, CRC Press Inc., 1998.
[33] R. Leonhardt, Dynamische Untersuchungen von Hydraulikkomponenten, Ph.D. thesis, Universität Karlsruhe, 2008.
[34] R.J. LeVeque, Balancing source terms and flux gradients in high-resolution Godunov methods: the quasi-steady wavepropagation algorithm, J. Comput. Phys. 146 (1998) 346–365.
[35] R.J. LeVeque, Finite Volume Methods for Hyperbolic Problems, Cambridge University Press, 2002.
[36] G.D. Maso, P. LeFloch, F. Murat, Definition and weak stability of nonconservative products, J. Math. Pures Appl. 74 (1995) 483–548.
[37] M. Muñoz, C. Parés, Godunov method for nonconservative hyperbolic systems, Math. Model. Numer. Anal. 41 (2007) 169–185.
[38] L. Müller, P. Blanco, A high order approximation of hyperbolic conservation laws in networks: application to one-dimensional blood flow, J. Comput. Phys. 300 (2015) 423–437.
[39] L. Müller, C. Parés, E. Toro, Well-balanced high-order numerical schemes for one-dimensional blood flow in vessels with varying mechanical properties, J. Comput. Phys. 242 (2013) 53–85.
[40] L. Müller, E. Toro, Well-balanced high-order solver for blood flow in networks of vessels with variable properties, Int. J. Numer. Methods Biomed. Eng. 29 (2013) 1388–1411.
[41] L. Müller, E. Toro, A global multiscale mathematical model for the human circulation with emphasis on the venous system, Int. J. Numer. Methods Biomed. Eng. 30 (2014) 681–725.
[42] S. Osher, F. Solomon, Upwind difference schemes for hyperbolic systems of conservation laws, Math. Comput. 38 (1982) 339–374.
[43] C. Parés, Numerical methods for nonconservative hyperbolic systems: a theoretical framework, SIAM J. Numer. Anal. 44 (2006) 300–321.
[44] D. Rochette, S. Clain, W. Bussière, Unsteady compressible flow in ducts with varying cross-section: comparison between the nonconservative Euler system and the axisymmetric flow model, Comput. Fluids 53 (2012) 53–78.
[45] E.F. Toro, Riemann Solvers and Numerical Methods for Fluid Dynamics, third edition, Springer, 2009.
[46] I. Toumi, A weak formulation of roe's approximate Riemann solver, J. Comput. Phys. 102 (1992) 360–373.
[47] W. Zielke, Frequency-dependent friction in transient pipe flow, J. Basic Eng. 90 (1968) 109–115.